# Condensation kinetics of microcavity polaritons with scattering by phonons and polaritons

T. D. Doan, Huy Thien Cao, and D. B. Tran Thoai
*Ho Chi Minh City Institute of Physics, Vietnam Center for Natural Science and Technology, 1 Mac Dinh Chi, Ho Chi Minh City, Vietnam*

H. Haug
*Institut für Theoretische Physik, J.W. Goethe-Universität Frankfurt, Max-von-Laue-Str. 1, D-60438 Frankfurt a.M., Germany*
(Received 23 March 2005; revised manuscript received 2 June 2005; published 1 August 2005)

We present numerical studies of the exciton polariton condensation kinetics in microcavities for the combined action of polariton-polariton and polariton-acoustic phonon scattering both for quasi-stationary and picosecond pulse excitation, respectively. For excitations of nearly resonant polaritons mainly the polariton-polariton scattering mechanism results in a condensation on the minimum of the lower polariton branch at relatively low areal polariton densities of the order of $10^9-10^{10}$ cm$^{-2}$. The simultaneously acting polariton-phonon scattering increases the number of condensed particles considerably by providing a heat dissipation from the polariton gas to the lattice. For nonresonant excitations at large $k$ values the considered scattering mechanisms cannot support a polariton condensation. Above (below) laser threshold there exists a (no) polariton condensate and the polariton distribution of the noncondensed particles can be fitted by a Bose-Einstein (Maxwell-Boltzmann) distribution. Our results for 3 ps pulse excitation are in very good agreement with recent experimental observations of Yamamoto *et al.*

DOI: 10.1103/PhysRevB.72.085301 PACS number(s): 71.35.−y, 73.20.Mf, 78.66.−w

## I. INTRODUCTION

The search for a boson condensation of excitons in semiconductors[1] has in recent years concentrated on the system of quantum well excitons in a microcavity. If the lowest photon mode in these cavities is nearly resonant with the lowest exciton level, the strong coupling provides well-resolved lower and upper branch polariton modes.[2] The system of polaritons which have to be pumped by optical excitation exhibits a laser threshold[3] due to the relaxation kinetics of the polaritons to the minimum of the lower polariton branch. Thus, the polariton lasing can be seen as a manifestation of a nonequilibrium bosonic condensation. The observed threshold polariton densities $n_{th}$ of the order of $10^9-10^{10}$ cm$^{-2}$ obey still the boson condition $n_{th}a_0^2 \ll 1$, where $a_0$ is the exciton Bohr radius of about 8 nm. Except for nonequilibrium effects this polariton condensation can also not be seen as a true Bose-Einstein condensation because the quantum well excitons as well as the photons of the lowest microcavity mode have only a transverse momentum. Two-dimensional systems lack a Bose-Einstein condensation at finite temperatures. A small cross section makes the transverse wave numbers discrete, which leads in particular to a gap between the lowest state and the next higher ones.[4,5] This energy gap in a finite 2D system leads again to a pronounced threshold behavior in the condensation kinetics. Naturally, if one wants to investigate a spontaneous condensation, one has to avoid coherent four-wave mixing effects in which a macroscopic population of the lowest polariton state is driven coherently by parametric optical amplification.[4,6] Thus the pumping has to be chosen in such a way that the excited polaritons lose their coherence with the exciting laser beam by scattering processes before they reach the lowest state. The basic two scattering mechanisms which are dominating the polariton condensation kinetics are the polariton-polariton (p-p) scattering[7] and the polariton-acoustic phonon (p-ph) scattering via the deformation potential coupling.[5,8] It has been noticed that in particular the less well-known heavy hole exciton deformation potential is so small in GaAs-type microcavities that the critical condensation densities due to p-ph scattering are considerably higher than those for p-p scattering.

As shown for the exciton condensation kinetics in Ref. 9 one should treat the population of the lowest state in which a condensation is expected separately with special care. We applied this technique together with the specifics of a 2D system with a finite cross section in our previous study of the microcavity polaritons due to the p-ph scattering mechanism.[5] We extend these studies here by including additionally the p-p scattering which has been analyzed by Tassone and Yamamoto[7] before. We rely on the boson approximation for the quantum well excitons, because in our studies we will stay at densities well below the saturation density at which the boson picture brakes down.

As in Ref. 5 we will include in our Boltzmann kinetics of the polariton distribution a time-dependent pump rate and the finite lifetime of the polaritons in the microcavity.[8] For the p-p scattering we will use the scattering rates of Ref. 7 and for the p-ph scattering we will use the formulations of Refs. 5 and 8. We will present results for the kinetics for the two scattering processes separately and jointly in order to study their specific contribution to the total kinetics.

One of the major results of our calculations is that the p-p scattering is mainly responsible for a condensation at critical densities of about $10^{10}$ cm$^{-2}$ in agreement with recent obser-

 

vations of Yamamoto *et al.*[3,10] The simultaneously acting p-ph scattering increases the condensate density and thus the intensity of the emitted laser light considerably, because they scatter already relaxed polaritons around the condensate state effectively into the lowest state. Differently from the p-p scattering, the p-ph scattering provides a heat dissipation mechanism by transferring at least parts of the optically introduced excess energy from the polariton gas to the cold lattice. This coupling to a heat sink is particularly important above the laser threshold, where the corresponding cooling allows an asymptotic approach of the chemical potential to zero with increasing total polariton density. Our studies show that this low threshold condensation only occurs for excitations of polaritons with small transverse momenta just above the bottleneck region, while an excitation of polaritons with large transverse momenta higher in the exciton-like part of the lower branch (nonresonant excitation) does not result in a condensation at polariton densities well below the saturation density, again in agreement with the experimental observations of Ref. 4. For the latter excitation conditions only laser action with the usual plasma gain has been observed at much higher threshold densities. Because the laser emission intensity is proportional to the polariton condensation density, time-resolved measurements[11,12] of the laser intensity after a short picosecond excitation pulse allow us to compare the buildup and decay of the polariton condensate with the calculated kinetics. Moreover one can probe again time-dependently the distribution of the noncondensed polaritons and compare these distributions with the calculated ones. The measured time-resolved properties, in particular the laser intensity and the resulting polariton distributions, are in very good agreement with the results of our polariton kinetics.

## II. RELAXATION KINETICS OF MICROCAVITY POLARITONS

In the following we will treat the polariton kinetics in microcavities (the spectrum and the Hopfield coefficient are given in the appendix) by using the semi-classical Boltzmann kinetics which has been used before in Refs. 13–15 to describe the exciton condensation kinetics and, e.g., in Refs. 5, 7, 8, 16, and 17 to investigate the 2D cavity polariton relaxation. We limit the rate equations for the population of the polariton states on the lower branch $f_{\vec{k}}(t)$ (an upper index is used if we refer to scattering into final states on the upper branch) and as mentioned before we will treat in addition the rate equation of the lowest states with the lowest momentum $\vec{k}_0$ with a population density $n_0(t)=f_0(t)/S$ separately. Here we write, e.g., $f_{\vec{k}_0}\rightarrow f_0$ for conciseness. The polariton rate equations have the form

$$\frac{\partial}{\partial t}f_{\vec{k}} = P_{\vec{k}}(t) - \frac{f_{\vec{k}}}{\tau_{\vec{k}}} + \left.\frac{\partial}{\partial t}f_{\vec{k}}\right|_{p\text{-}p} + \left.\frac{\partial}{\partial t}f_{\vec{k}}\right|_{p\text{-}ph}, \tag{1}$$

$$\frac{\partial}{\partial t}n_0 = -\frac{n_0}{\tau_0} + \left.\frac{\partial}{\partial t}n_0\right|_{p\text{-}p} + \left.\frac{\partial}{\partial t}n_0\right|_{p\text{-}ph}. \tag{2}$$

Here, $P_{\vec{k}}(t)$ is the time-dependent pump rate and $\tau_{\vec{k}}$ is the polariton lifetime.[8] For the decay rate $1/\tau_k^i$, we use the same approximation as given by Bloch and Marzin for a GaAs quantum well:[8] $1/\tau_k=(v_k)^2/\tau^c$ for $0<k<k_{cav}=6\times10^4$ cm$^{-1}$; $1/\tau_k=1/\tau^x$ for $k_{cav}<k<k_{rad}=n_{cav}E_0^x/\hbar c=2.3\times10^5$ cm$^{-1}$; and $1/\tau_k=0$ for $k>k_{rad}$; $\tau^c$ and $\tau^x$ are the radiative lifetimes of photons and excitons, respectively; $v_k^2=1-u_k^2$ is the photon Hopfield coefficient of the lower branch. In this form of the rate equation the necessity to keep the cross section finite has two reasons: First, only with a finite $S$ a well-defined condensation occurs,[5] and second only with a finite $S$ are the spontaneous transition rates into the condensate maintained which initiate the condensation.[13] The p-p scattering rates have the basic form

$$\left.\frac{\partial}{\partial t}f_{\vec{k}}\right|_{p\text{-}p} = -\sum_{\vec{k}',\vec{k}_1,\vec{k}_2} w^{p\text{-}p}_{\vec{k},\vec{k}',\vec{k}_1,\vec{k}_2}[f_{\vec{k}}f_{\vec{k}'}(1+f_{\vec{k}_1})(1+f_{\vec{k}_2}) - f_{\vec{k}_1}f_{\vec{k}_2}(1+f_{\vec{k}})(1+f_{\vec{k}'})], \tag{3}$$

where $\vec{k}_1=\vec{k}+\vec{q}$ and $\vec{k}_2=\vec{k}'-\vec{q}$. The transition probability $w^{p\text{-}p}$ is determined by the Coulomb exchange interaction between two excitons. The transition probability has been analyzed by Tassone and Yamamoto[7] for the given situation by taking into account the scattering processes in which all states are on the lower branch as well as for situations in which one of the lower branch polaritons is scattered into the upper branch. We use here the form of the p-p transition probability of Ref. 7. In an isotropic approximation the transition probability is

$$W^{p\text{-}p}_{k,k';k_1,k_2} = \frac{\pi}{\hbar}\frac{S^2}{(2\pi)^4}\frac{\Delta E^2|M|^2u_k^2u_{k'}^2u_{k_1}^2u_{k_2}^2}{\frac{\partial E(k')}{\partial k'^2}\frac{\partial E(k_1)}{\partial k_1^2}\frac{\partial E(k_2)}{\partial k_2^2}}R(k,k',k_1,k_2). \tag{4}$$

The exchange interaction matrix element is estimated in the limit of small momentum transfer by

$$M \simeq 2\sum_{k,k'} V_{\vec{k}-\vec{k}'}\varphi_k\varphi'_k(\varphi_k^2-\varphi_k\varphi_{k'}) \simeq 6E_0\frac{a_o^2}{S}, \tag{5}$$

where $\varphi_k$, $E_0$, and $a_0$ are the 2D 1$s$ exciton wave function, the binding energy, and the Bohr radius, respectively. $V_k=2\pi/(Sk)$ is the 2D Coulomb potential. The estimated exciton-exciton interaction matrix element of $6E_0(a_o^2/S)$ is often used in 2D systems. The terms proportional to the 2D density of states $\partial E(k')/\partial k'^2$ stem from a transition from the momentum integration to the energy summation. The term $R$ finally is given by

$$R(k,k',k_1,k_2) = \int \frac{dq^2}{\sqrt{[(k+k_1)^2-q^2][q^2-(k-k_1)^2][(k'+k_2)^2-q^2][q^2-(k'-k_2)^2]}}. \quad (6)$$

The $q^2$ integration has to be taken over the range in which all four terms under the square root are non-negative. The energy conservation is built in if one takes $k_2=k(E_2=E_k+E_{k'}-E_{k_1})$ and sums over the $k'$ and $k_1$. Consistently with Eq. (2) one has to single out the transitions in which one of the wave numbers $k'$, $k_1$, or $k_2$ is equal to $k_0$. In these scattering rates between the continuum and the condensate state one introduces as in (2) $f_0(t)=n_0(t)S$. The transition probabilities due to the scattering by acoustic phonons can be written as

$$W_{\vec{k},\vec{k'}} = \frac{L_z(u_k u_{k'}\Delta_{k,k'})^2}{\hbar\rho V u^2 q_z} B^2(q_z) D^2(|\vec{k}-\vec{k'}|) N^{ph}_{E_{k'}-E_k}\theta \times(\Delta_{k,k'}-|\vec{k}-\vec{k'}|), \quad (7)$$

where

$$\Delta_{k,k'} = \frac{|E_{k'}-E_k|}{\hbar u}, \quad (8)$$

$$q_z = [(\Delta_{k,k'})^2 - |\vec{k}-\vec{k'}|^2]^{1/2}, \quad (9)$$

$$D(q) = D_e F\left(\frac{qm_h}{m_e+m_h}\right) - D_h F\left(\frac{qm_e}{m_e+m_h}\right), \quad (10)$$

$$B(q) = \frac{8\pi^2}{L_z q(4\pi^2 - L_z^2 q^2)} \sin\left(\frac{L_z q}{2}\right), \quad (11)$$

$$F(q) = [1+(qa_0/2)^2]^{-3/2}. \quad (12)$$

Here $L_z$ is the quantum well width, $F(q)$ is proportional to the 2D exciton wave function, the effective mass ratios in (10) pick out the $e,h$ momenta of the relative motion, respectively, $V$ is the crystal volume, $u$ is the longitudinal sound velocity, $\rho$ is the mass density of the solid, and $D_{e(h)}$ are the deformation potentials. $N_E^{ph}$ is the thermal phonon population factor for the phonon absorption or emission. For $E>0$ $N_E^{ph}$ is equal to the Bose distribution $n_{E=\hbar\omega}$ (absorption) and for negative energies equal to $n_{E=\hbar\omega}+1$ (emission). $D_e$,$D_h$ are the electron and heavy hole deformation potentials.

Again the separation of the transitions between the continuum and the condensate has to be performed as before (for details see Ref. 5).

Before we present results, we list the used material parameters for GaAs-type quantum wells and microcavities:[5,8,18,19] $E_0^x=1.515$ eV, $m_e=0.067m_0$, $m_h=0.45m_0$, $a_{2D}=10$ nm, the index of refraction $n_{\rm cav}=3.43$, the cavity Rabi splitting $\hbar\Omega=5$ meV, the deformation potentials $D_e=-8.6$ eV, $D_h=5.7$ eV,[12] $u=4.81\times10^5$ cm s$^{-1}$, and $\rho=5.3\times10^3$ kg m$^{-3}$. Particularly the value of the heavy-hole deformation potential is fluctuating in the literature, therefore we also use the smaller value of $D_h=3.5$ eV in some of the presented calculations. The influence of its precise value on the relaxation kinetics has been studied in detail in Ref. 5. The microcavity cross section will be taken as $S=100$ $\mu$m$^2$ and the quantum well width as $L_z=5$ nm. The lifetimes are assumed to be $\tau^x=20$ ps and $\tau^c=8$ ps. The bath temperature is varied between $T=4$ and 10 K. The detuning is defined as $\delta=E_0^c-E_0^x$ and will be varied between 0 and 6 eV. For the quasi-stationary pump rate we will use the form $P_k(t)=P_k\tanh(t/t_0)$ with $t_0=50$ ps in order to reach stationary equilibrium. The pumping creates polaritons around the wave number $k_p$ with the distribution $P_k=P_0 e^{-\hbar^2(k-k_p)^2/2m_x\Delta E}$. The width is $\Delta E=0.1$ meV. We will study near-resonant and off-resonant pumping. For near-resonant pumping polaritons are excited just above the bottleneck, but with a wave number still large enough to avoid coherent parametric scattering into the lowest state. In this case the pumping is centered at $k_p=1.7\times10^5$ cm$^{-1}$. For nonresonant pumping we assume pumping at a large wave number $k_p=4.85\times10^6$ cm$^{-1}$ well on the excitonic part of the dispersion.

For pulse excitation we use as in the corresponding experiments[3] a Gaussian pulse of the form $P_k(t)=P_k\exp[-2\ln 2(t/t_p)^2]$ with a pulse width of $t_p=3$ ps.

## III. NUMERICAL RESULTS

### A. Quasi-stationary pumping

First we will examine the kinetics of the condensate fraction $n_0(t)/n_{tot}$ with a smoothly switched on stationary excitation. Here $n_{tot}$ is the stationary total density for the chosen

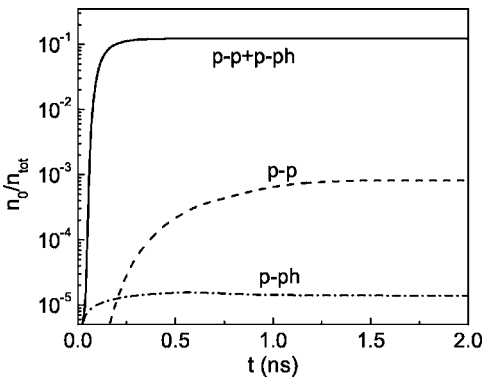


FIG. 1. Calculated condensate fraction $n_0(t)/n_{tot}$ for quasi-stationary near-resonant pumping for various scattering mechanisms. The bath temperature is $T=4$ K and the detuning in the microcavity is zero. The total stationary polariton density is $n_{tot}=3.96\times10^{10}$ cm$^{-2}$. Full line: p-p and p-ph scattering, the resulting condensate population is $f_0=n_0S=4.84\times10^3\gg1$. Dashed line: only p-p scattering, $f_0=3.15\times10^1>1$. Dashed-dotted line: only p-ph scattering, $f_0=5.58\times10^{-1}<1$.

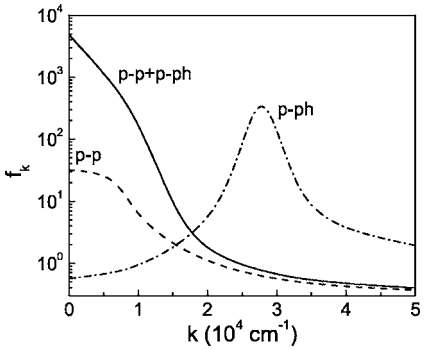


FIG. 2. Calculated stationary distribution function for the noncondensed polaritons for the parameters and the scattering mechanisms of Fig. 1.

excitation together with the resulting polariton distributions. We compare the results for near resonant and nonresonant excitation. The total polariton density is used as a measure of the pump strength. In these studies we will compare additionally the resulting kinetics due to the two individual scattering mechanisms and due to the combined one. We start with the stationary, near-resonant excitations of excitons slightly above the bottleneck region.

In Fig. 1 the evolution of the condensate fraction is shown for the phonon (p-ph) scattering (dashed-dotted line) and the polariton (p-p) scattering (dashed line) alone. For p-ph scattering a condensation is not reached, while for p-p scattering the threshold of condensation is reached with $f_0=n_0S\simeq 30$. The kinetics due to both scattering processes (full line) results in a strong condensation with a large stationary value of the condensate population $f_0=1.73\times 10^3\gg 1$.

Next we will show the asymptotically reached distributions of noncondensed polaritons in Fig. 2. Consistent with the condensate fraction, we see that the distribution for the p-ph scattering is still nondegenerate, while the distribution for the p-p scattering already piles up near the lowest energy values. For the combined action of both scattering processes (full line) degenerate polariton distribution is obtained. The

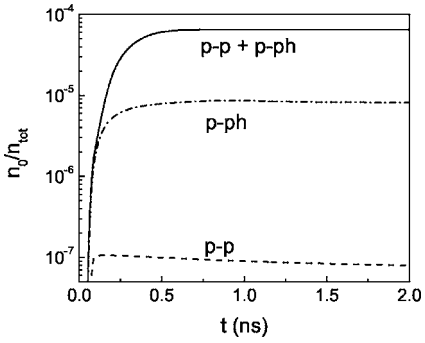


FIG. 3. Calculated condensate fraction $n_0(t)/n_{tot}$ for quasistationary off-resonant pumping for various scattering mechanisms. The bath temperature is $T=4$ K and the MC detuning is zero. The total stationary polariton density is nearly the same as in Fig. 1, namely $n_{tot}=4.1\times 10^{10}$ cm$^{-2}$. Full line: p-p+p-ph scattering, the resulting condensate population is $f_0=n_0S=2.44$. Dashed line: only p-p scattering, $f_0=3.1\times 10^{-3}\ll 1$. Dashed-dotted line: only p-ph scattering, $f_0=0.35$.

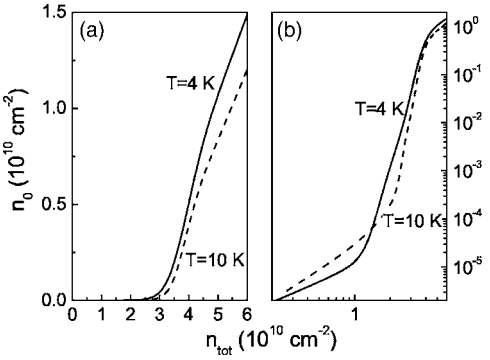


FIG. 4. Calculated condensate density $n_0(t)$ versus the total polariton density $n_{tot}$ for near-resonant pumping and the combined p-p+p-ph scattering for two bath temperatures of $T=4$ K (full line) and $T=10$ K (dashed line). Left: linear scale, right: logarithmic scale.

polaritons accumulated by the p-p scattering at low energies are scattered into the condensate by the p-ph scattering mechanism.

We compare these results with the ones for nonresonant pumping with a similar total polariton density shown in Fig. 3. We see that for nonresonant pumping a condensation with $f_0\gg 1$ is not achieved as it has been observed in the experiment,[3,11] where laser action has only been obtained for the case of near-resonant excitation.

In order to study the sharpness of the condensation and laser threshold and its temperature dependence we plot the asymptotically established condensate density versus the total density in Fig. 4, which serves as a measure for the pump strength for the nearly resonant excitation. In the logarithmic plot (right-hand side of Fig. 4) the characteristic s-shape of a nonequilibrium phase transition shows up clearly.

In Fig. 5 we show the influence of the detuning $\delta$ for the combined p-p and p-ph scattering kinetics for the bath temperature of $T=4$ K.

As already studied in Ref. 5 for the p-ph scattering kinetics, one can lower the threshold of condensation to a certain extent by increasing the exciton component of the lower branch polaritons by increasing the detuning. Figure 5 shows this statement holds also for the combined kinetics of both scattering mechanisms at $T=4$ K.

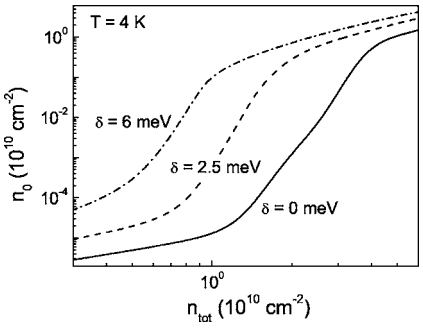


FIG. 5. Calculated condensate density $n_0(t)$ versus the total polariton density $n_{tot}$ for near-resonant pumping and the combined p-p+p-ph scattering for the bath temperatures of $T=4$ K for various values of the detuning: $\delta=0$ meV (full line), $\delta=2.5$ meV (dashed line), $\delta=6$ meV (dashed-dotted line).

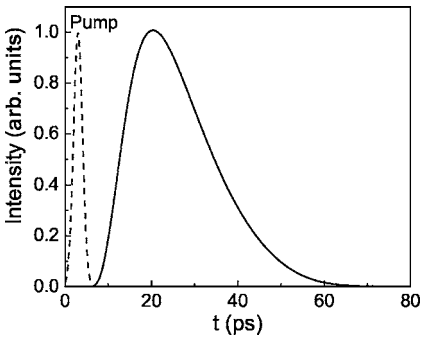


FIG. 6. The buildup and decay of the condensate $n_0(t)$ after a 3 ps pump pulse which is shown by the dashed curve. The total polariton density after the pulse has been above threshold $n_{tot}/n_{th}=1.3$ with $n_{th}=5\times10^9$ cm$^{-2}$.

### B. Pulse excitation

In order be able to compare our findings directly with the experimental results,[3,10–12] we, as in the experiment, use a nearly resonant pulse excitation with a pulse width of $t_p=3$ ps. For this short pulse excitation the faster p-p scattering determines again the initial relaxation into the condensate state, while the slower p-ph interaction is important for the cooling of the polariton gas into a nearly degenerate distribution. The calculated buildup of the condensate population after a 3 ps pulse with a peak pump strength of $P_0=0.65$ is shown in Fig. 6.

For the supercritical pump rate $P/P_{th}=1.75$ (which is higher above threshold compared to the pump rate $n_{tot}/n_{th}=1.3$ of Fig. 6) the laser intensity reaches a peak roughly 10 ps after the excitation pulse. Because the laser output is proportional to the condensate population, one can compare it with the measured laser intensity.[3,10–12] We show for comparison the measured output in the laser mode versus time (see Fig. 7) after a 3 ps excitation pulses.[10]

The observed delay of the output with respect to the pump pulse and dynamics of the output pulse is similar to the calculated population kinetics of the condensate as shown in Fig. 6. Because we did not try to model details of the experimentally used microstructures a more quantitative comparison would not be appropriate.

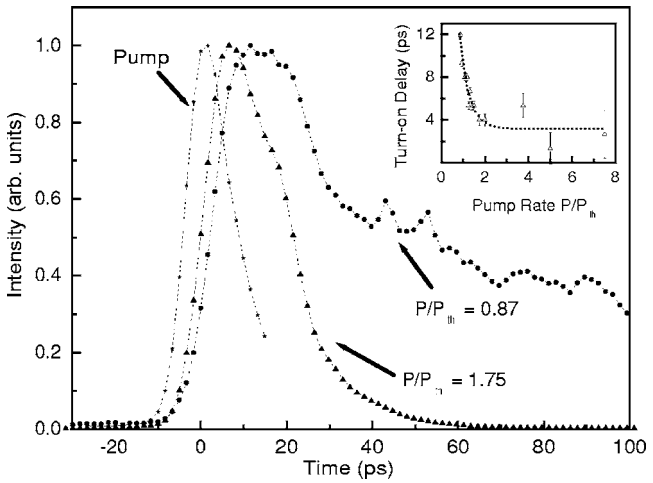


FIG. 7. The buildup and decay of the measured output in the laser mode above and below threshold at the pump powers $P/P_{th}=1.75$ and $P/P_{th}=0.87$, respectively, according to Ref. 10.

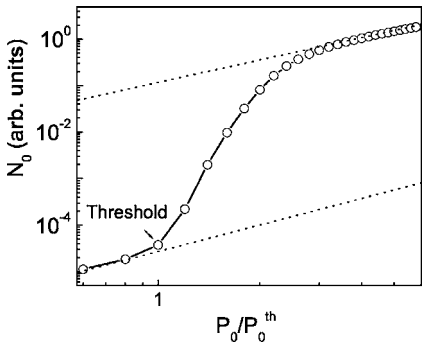


FIG. 8. The time-integrated condensate density $N_0=\int dt' n_0(t')$ versus the normalized total pump power $P_0/P_0^{th}$. The threshold density estimated from this plot is $n_{th}=5\times10^9$ cm$^{-2}$.

The threshold scenario is seen by plotting the time-integrated condensate density versus the total pump rate in Fig. 8 with an areal threshold polariton density of $n_{th}=5\times10^9$ cm$^{-2}$.

As Fig. 9 shows, experimentally[12] one has found a rather similar dependence of the integrated laser output on the polariton density around the laser threshold and a very similar polariton threshold density.

At the peak of the condensate density the polariton distribution over finite $k$ values is not yet in thermal equilibrium. Particularly below threshold one has to wait long before the polariton gas can be fitted reasonably well with a nondegenerate Maxwell-Boltzmann distribution. For supercritical conditions one can fit the resulting polariton distribution with a Bose-Einstein distribution about 50 ps after the pump pulse as shown in Fig. 10. Generally speaking, the thermalization becomes faster the higher the total polariton densities are.

The chemical potential and temperature obtained from the fits are shown in Figs. 11 and 12.

The ratio of the chemical potential to the temperature is seen to approach zero asymptotically high above threshold.

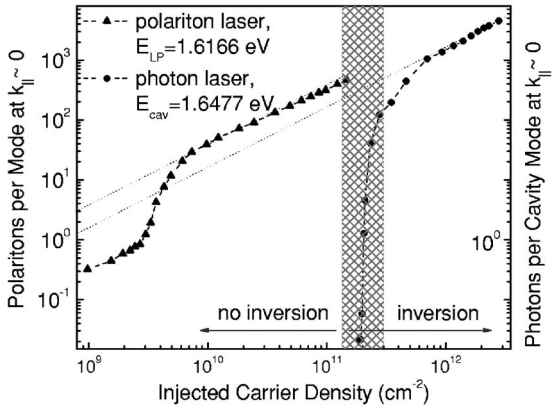


FIG. 9. The measured laser intensity for the polariton laser versus the excited polariton density (left curve). The right curve shows the usual e-h-plasma laser intensity obtained under nonresonant excitation at a much higher threshold density according to Ref. 12.

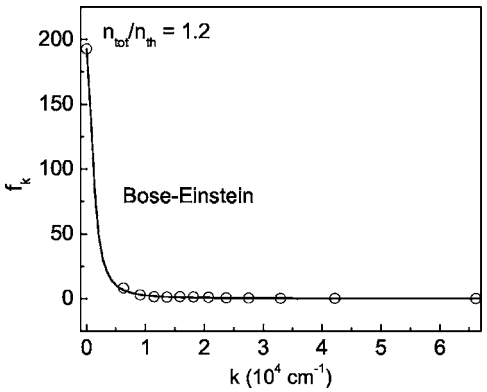


FIG. 10. For supercritical conditions $n_{tot}/n_{th}=1.2$ the polariton distribution function can be fitted to a degenerate Bose-Einstein distribution at the time of 50 ps after the pulse.

This asymptotic approach occurs only in the presence of the cooling due to the polariton-phonon scattering which takes away the excess energy introduced by the nonresonant optical pumping. The resulting heating in the polariton gas is shown in Fig. 12. One sees a clear saturation of the thermal energy at higher densities, which allows the asymptotic approach of the chemical potential to zero even under pulse excitation conditions.

Again this scenario is found also in the measured polariton distribution. The measured distribution too can be fitted to a Bose-Einstein distribution. Figure 13 shows that the resulting chemical potential and temperature show qualitatively the same behavior as the calculated ones, although with a stronger heating in comparison with the numerical simulations.

All our results for the 3 ps pulse excitation are in good qualitative agreement with the observations of Yamamoto *et al.* for comparable excitation conditions. In particular they fully support the interpretation of the polariton lasing in terms of a nonequilibrium bosonic condensation.

In conclusion, we have shown that for nearly resonant excitation just above the bottleneck the polariton kinetics results in a polariton condensation at sufficiently low polariton densities. For nonresonant excitation of energetically higher exciton states the kinetics does not yield a condensation for densities below the saturation density, where the exciton boson picture breaks down. For nearly resonant excitation mainly the polariton-polariton scattering is responsible for achieving this low threshold concentration, but the polariton-phonon scattering increases the number of condensed particles considerably, because this mechanism scatters the polaritons piled up around the condensate state into it. For bath temperature below 10 K the obtained threshold concentration is of the order of $5\times10^9$ cm$^{-2}$. For a 3 ps near-resonant pulse excitation as it has been used in the experiments of Yamamoto *et al.*, we have shown that above

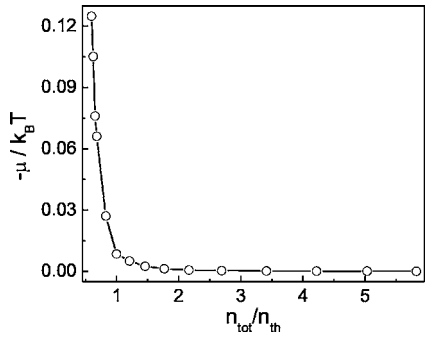


FIG. 11. The ratio of the chemical potential to the thermal energy resulting from the fits of supercritical distributions to a Bose-Einstein distribution versus the normalized total polariton density $n_{tot}/n_{th}$.

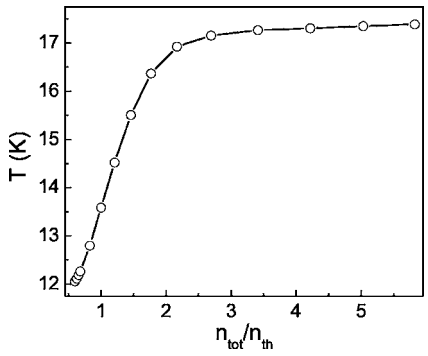


FIG. 12. The thermal energy of the polariton gas obtained from the fits of supercritical distributions to a Bose-Einstein distribution versus the normalized total polariton density $n_{tot}/n_{th}$.

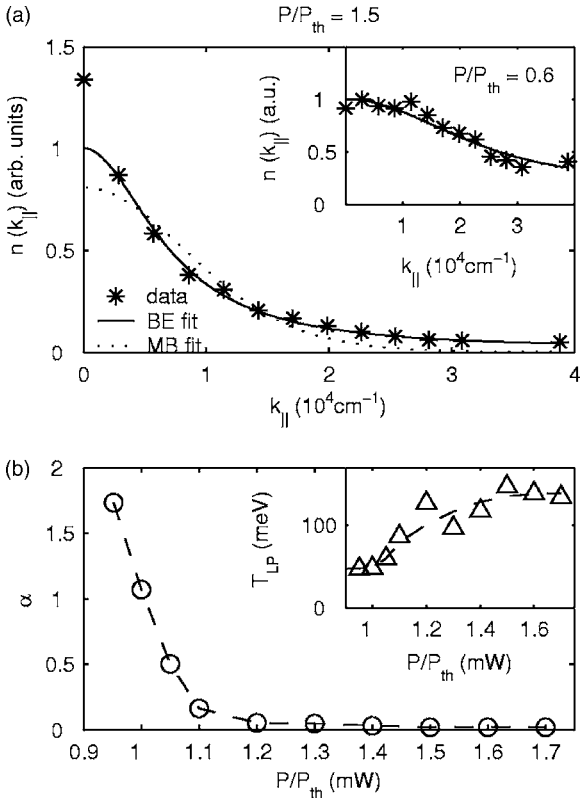


FIG. 13. Fit of the Bose-Einstein distribution to the measured polariton distribution (top part). The lower part shows the variation of the chemical potential and the temperature with the pump power normalized to the threshold density according to Ref. 3.

threshold the distribution of the noncondensed polaritons is a Bose-Einstein distribution. The resulting chemical potential approaches zero as the pump intensity increases well above threshold. Simultaneously the polariton gas heats up. The condensate population reaches large values above the laser threshold. All these findings are in good qualitative agreement with experimental observations by Yamamoto *et al.*[3,10] and confirm the interpretation of the microcavity polariton lasing as a clear signature of a nonequilibrium bosonic condensation. A detailed test of the considered polariton condensate kinetics in terms of $n_0(t)$ has been carried out by comparing it with the measured laser intensity $I(t)$ which is proportional to $n_0(t)$ after a short picosecond excitation pulse. The good quantitative agreement between the calculated $n_0(t)$ and the measured $I(t)$ shows that the considered kinetic model in terms of polariton-polariton and polariton-acoustic phonon scattering gives a rather accurate description of the polariton condensation and laser kinetics in quantum well microcavities.


## ACKNOWLEDGEMENTS

Two of us (H.T.C., D.B.T.T.) gratefully acknowledge the financial support of the National Program for Basic Research. We are grateful to Y. Yamamoto, G. Weihs, and H. Deng for allowing us the reprint of their experimental results.


## APPENDIX: MICROCAVITY POLARITON DISPERSION

Within the two-coupled band model (considering only the 1*s* state of the heavy-hole quantum well excitons), the energies for the upper and lower cavity polariton branches are given by[8,17]

$$E_k^{+(-)} = \frac{1}{2}[E_k^c + E_k^x \pm \sqrt{(E_k^c - E_k^x)^2 + (\hbar\Omega)^2}], \tag{A1}$$

where

$$E_k^c = \frac{\hbar c}{n_{cav}}\left(\frac{\pi}{L_c} + k^2\right)^{1/2}, \tag{A2}$$

$$E_k^x = E_0^x + \frac{\hbar^2 k^2}{2(m_e + m_h)}. \tag{A3}$$

Here $E_0^x$ is the fundamental exciton energy, $m_e$ ($m_h$) is the electron (hole) in-plane mass, $n_{cav}$ is the cavity refraction index, $L_c$ is the cavity length, $\Omega$ is the Rabi splitting, and $k$ is the 2D momentum wave number. For GaAs parameters the rather flat part of the polariton spectrum where the exciton and photon mix strongly ends at a wave number of $k \simeq 2 \times 10^4$ cm$^{-1}$. This wave number defines the position of the bottleneck region.

The corresponding Hopfield coefficients for the transformation of polariton operators of branch $i$ ($\alpha_{\vec{k}}^i$) from excitons ($a_{\vec{k}}$) and photons ($b_{\vec{k}}$) with $\alpha_{\vec{k}}^i = u_k^i a_{\vec{k}} + v_k^i b_{\vec{k}}$, with $(u_k^i)^2 + (v_k^i)^2 = 1$ are

$$u_k^i = \pm \frac{1}{\sqrt{1 + \left(\frac{\Omega/2}{E_k^i - E_k^x}\right)^2}}. \tag{A4}$$

Note that the exciton Hopfield coefficients are finite when $k \to 0$ so that the bottleneck effect is strongly reduced in a microcavity. A finite positive detuning increases the exciton component on the lower branch particularly in the region of low momenta.

A finite cross section will make the spectrum of the momenta discrete $k_{n_i,i} = n_1(\pi/L_1)$ with $n_i = 1,2,3,...$ and $S = L_x L_y$.


[1] S. A. Moskalenko and D. W. Snoke, *Bose-Einstein Condensation of Excitons and Biexcitons* (Cambridge University Press, Cambridge, 2000).

[2] C. Weisbuch, M. Nishioka, A. Ishikawa, and Y. Arakawa, Phys. Rev. Lett. **69**, 3314 (1992).

[3] H. Deng, G. Weihs, D. Snoke, J. Bloch, and Y. Yamamoto, Proc. Natl. Acad. Sci. U.S.A. **100**, 15318 (2003).

[4] D. Porras, C. Ciuti, J. J. Baumberg, and C. Tejedor, Phys. Rev. B **66**, 085304 (2002).

[5] H. T. Cao, T. D. Doan, D. B. Tran Thoai, and H. Haug, Phys. Rev. B **69**, 245325 (2004).

[6] P. G. Savvidis, J. J. Baumberg, R. M. Stevenson, M. S. Skolnick, D. M. Whittaker, and J. S. Roberts, Phys. Rev. Lett. **84**, 1547 (2000).

[7] F. Tassone and Y. Yamamoto, Phys. Rev. B **59**, 10830 (1999).

[8] J. Bloch and J. Y. Marzin, Phys. Rev. B **56**, 2103 (1997).

[9] O. M. Schmitt, D. B. Tran Thoai, L. Banyai, P. Gartner, and H. Haug, Phys. Rev. Lett. **86**, 3839 (2001).

[10] H. Deng, G. Weihs, C. Santori, J. Bloch, and Y. Yamamaoto, Science **298**, 199 (2002).

[11] G. Weihs, H. Deng, D. Snoke, and Y. Yamamoto, Phys. Status Solidi A **201**, 625 (2004).

[12] G. Weihs, H. Deng, R. Huang, M. Sugita, F. Tassone, and Y. Yamamoto, Semicond. Sci. Technol. **18**, S386 (2003).

[13] L. Banyai, P. Gartner, O. M. Schmitt, and H. Haug, Phys. Rev. B **61**, 8823 (2000).

[14] D. B. Tran Thoai and H. Haug, Solid State Commun. **115**, 379 (2000).

[15] L. Banyai and P. Gartner, Phys. Rev. Lett. **88**, 210404 (2002).

[16] F. Tassone, C. Piermarocchi, V. Savona, A. Quattropani, and P. Schwendimann, Phys. Rev. B **53**, R7642 (1996).

[17] F. Tassone, C. Piermarocchi, V. Savona, A. Quattropani, and P. Schwendimann, Phys. Rev. B **56**, 7554 (1997).

[18] S. Pau, G. Bjork, J. Jacobson, H. Cao, and Y. Yamamoto, Phys. Rev. B **51**, 7090 (1995).

[19] U. Bockelmann, Phys. Rev. B **48**, 17637 (1993).